Global climate-driven trade-offs between the water retention and cooling benefits of urban greening

Authors: M. O. Cuthbert[1,2]*, G. C. Rau[2,3], M. Ekström[1], D. M O'Carroll[2], A. J. Bates[4].

Affiliations:

[1]School of Earth and Environmental Sciences, Cardiff University, Cardiff, UK.

[2]School of Civil and Environmental Engineering, The University of New South Wales, Sydney, Australia.

[3]Institute of Applied Geosciences, Karlsruhe Institute of Technology, Karlsruhe, Germany.

[4]School of Animal, Rural & Environmental Sciences, Nottingham Trent University, Nottingham, UK.

*Correspondence to: cuthbertm2@cardiff.ac.uk

Abstract

Heat-related mortality and flooding are pressing challenges for the >4 billion urban population worldwide, exacerbated by increasing urbanization and climate change. Urban greening, such as green roofs and parks, can potentially help address both problems, but the geographical variation of the relative hydrological and thermal performance benefits of such interventions are unknown. Here we quantify globally how climate driven trade-offs exist between modelled hydrological retention and cooling potential of urban greening. Water retention generally increases with aridity in water limited environments, while cooling potential favors lower aridity, energy limited, climates. Urban greening cannot yield high performance simultaneously for addressing both urban heat-island and urban flooding problems in most cities globally. However, in more arid locations, where sustainable, irrigation might be used to improve potential cooling benefits while maintaining retention performance. We demonstrate that as precipitation becomes increasingly variable with climate change, the hydrological and thermal performance of thinner substrates would both diminish more quickly compared to thicker and more deeply vegetated systems, presenting challenges for urban greening strategies. Our results provide a conceptual framework and geographically targeted quantitative guide for urban development, renewal and policymaking.

Introduction

Cities are hot spots for future population increase and already home to more than 55% of the 7.6 billion global population[1]. Urban areas also have unique climates, re-shaping local water and energy budgets relative to peri-urban and rural environments. Well known urban climate risks are the urban heat island (UHI) effect where a city's unique signature of sensible and latent heat fluxes combine to enhance warming[2-4]. In addition, the urban stream syndrome (USS) reflects the widely reported degraded physical, chemical, and biological conditions caused by urbanization of watersheds[5-7]. In combination, these present pressing water management and health challenges associated with substantial financial (e.g. infrastructure) and social (e.g. human wellbeing and mortality) risks, and increasingly so under climate change[8,9].

To combat these problems, a commonly proposed strategy for urban development and renewal[10] is to increase the proportion of 'urban greening' in the form of green roofs, green walls or vegetated urban ground surfaces[11,12]. This can potentially reduce the UHI and USS and support local ecosystem services and resident wellbeing[13]. Owing to the multiplicity of potential advantages and disadvantages associated with green surfaces, multidisciplinary studies have been used to assess their overall value[14]. The mitigation of the stormwater retention component of the USS and the UHI effect are reported to be the most important associated benefits and opportunities respectively[15].

Antecedent conditions strongly influence the ability of vegetated surfaces to delay and reduce run-off generation. The maximum ability of a vegetated surface to retain water during and after rainfall requires a period of relatively dry conditions preceding a rainfall event. This enables more potential storage to accumulate in the pores of the substrate/soil layer[16], driven by loss of soil moisture back to the atmosphere. Cooling due to urban greening also occurs predominantly via increased evapotranspiration[6,7] but requires consistently moist conditions either from precipitation or irrigation, along with a significant potential evaporation demand. Despite the overall similarities in the driving processes for potential retention and cooling, no large-scale studies have systematically addressed the assessment of these combined environmental benefits or their relative performance across different climatic regions.

Here we propose a conceptual and data-driven framework to understand and quantitatively estimate the comparative retention and cooling potential of urban greening globally. The internal consistency of data and methods enable a visualization of global patterns in the efficacy of cooling and retention solutions. The analysis exposes both regional solutions and a requirement to trade-off the adaptive functionality of urban greening to address either excess warming or flooding, depending on the prevailing climate. Adequate local-scale information is not yet available in most locations globally to support urban development policy. Our results thus provide a much needed first-order, coarse-grained, geographic foundation for decision-making guidance to policy makers. The results can be used to broadly scope the potential of urban greening to mitigate for heat and flood related climate risks. This is particularly valuable where local-scale information is unavailable.

Results

Aridity controlled retention-cooling trade-offs

We applied a parsimonious hydrological model (Figure S1,S2) worldwide using daily forcing precipitation (P) and potential evapotranspiration (PET) derived from re-analysis data[17] to derive gridded global outputs (Figure S3,S4). We then extracted modelled outputs for the locations of 31 500 urban areas globally from the Global Rural-Urban Mapping Project (GRUMP)[18]. To assess differences in modelled output using gridded and point forcing data, an additional suite of models was run using meteorological data from the Global Surface Summary of the Day (GSOD)[19] archive for 175 cities that contain precipitation measurements of sufficient quality and duration (see locations in Figure 1B,1E). Three urban greening types were modelled, representing extensive (depth h = 50 mm), intensive (h = 150 mm) and deep (h = 1 000 mm) substrates using parameters appropriate for typical, well drained, engineered green surfaces. Irrigated scenarios were also explored for the intensive substrate. We used Monte Carlo experiments to resolve the parameter equifinality of the model in order to constrain the uncertainty in limiting our global results to a limited number of parameter sets. The model simulates drainage (D) which can be used to determine hydrological retention when aggregated on a long term mean basis as (P-D)/P. Since the model also generates estimations of actual evapotranspiration (AET) which is the dominant driver for urban cooling[6,7], we also derive and evaluate a semi-empirical potential cooling metric (AET/PET). This model can explain >70% of the variance in global mean UHI data[20,21] with climate for large cities (Figure S5). In combination, these dimensionless metrics thus represent a practical way of approximating the relative potential performance of retention and cooling for different urban greening interventions at any given location, or the same urban greening intervention at different locations.

Here we make the novel observation that the equation for mean retention can be expressed in identical terms as the Budyko curve[22] ordinate axis (AET/P). This leads logically to using the Budyko hypothesis as a framework in which to analyze the results and generalize the controls on the hydrological performance. The climate metric of relevance as the dependent variable in our analysis then becomes the abscissa of the Budyko relation (PET/P) which is also the inverse of the aridity index (P/PET). We show that the application of the Budyko framework in this way is a powerful tool for explaining the overall trade-off between cooling and retention as follows, with reference to our results for the intensive substrate (Figure 1).

Towards the left side of sub-panels C and F in Figure 1 where PET/P<1, conditions are defined as 'energy limited' since there is more than enough precipitation to meet the energy demands of the atmosphere driving evapotranspiration. In such an environment the retention capacity is lowest since only a proportion of the precipitation can be evaporated and drainage rates will be high from the excess precipitation available. However, cooling is principally driven by the change of sensible to latent heat during evaporation. Hence, the highest rates of cooling potential are found in the energy limited part of the Budyko curve. This is consistent with the overall shape of global UHI observations as should be expected (Figure S5).

In contrast as we move towards the right side of Budyko space where PET/P>1, conditions are 'water limited' since there is a limited amount of water available (P) for evapotranspiration (AET) despite the high potential evaporative demand from the atmosphere (PET). At this end of the Budyko curve we have higher rates of AET as a proportion of P leading to higher retention rates. But at the same time the relative amount of AET as a proportion of the overall energy budget is decreasing so the rates of relative cooling potential decrease. The general pattern is thus that, in broad terms, energy limited climates favor cooling

more than retention, whereas water limited climates favor retention more that cooling. However, there are many important and interesting variations within this overall pattern that can be quantified from our results.
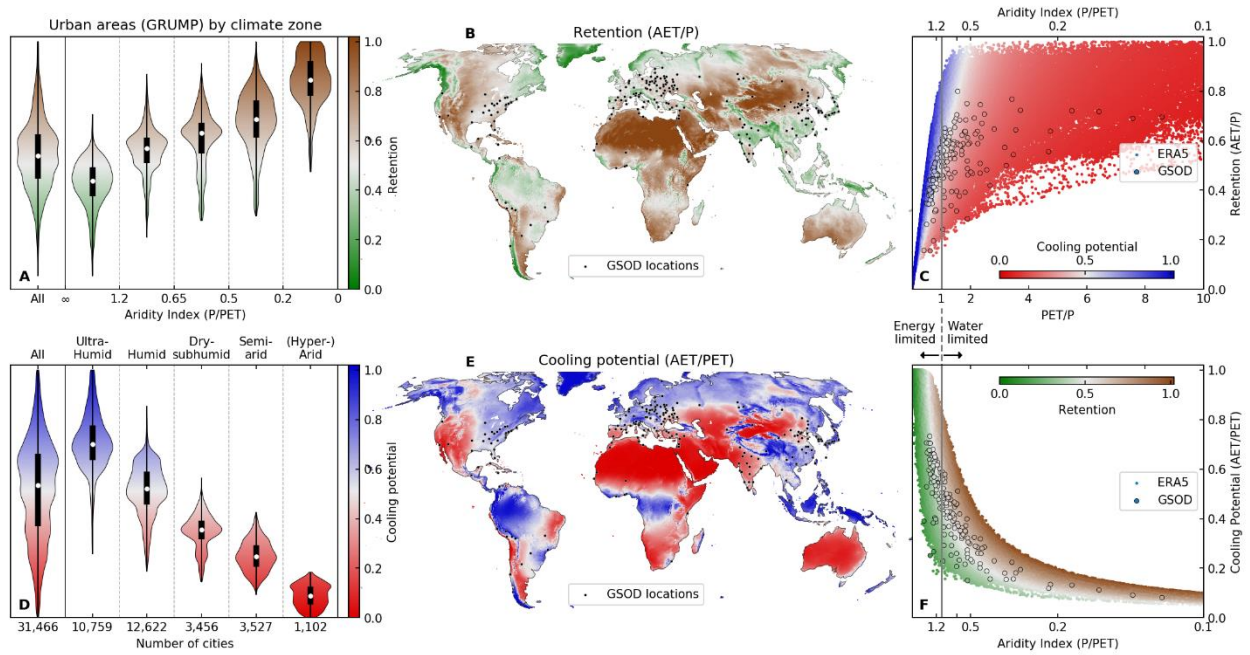

Figure 1. Global patterns of urban greening hydrological retention and cooling potential. Spatial distributions and interrelationships of ERA5 re-analysis data forced models using 'intensive substrate' (h = 150 mm) for: (B, C) Retention and (E, F) Cooling potential. (A, D) Violin plots for data extracted from GRUMP[18] urban areas only. GSOD[19] city point-data and locations are shown for reference in (B, C) and (E, F).

Influence of substrate choice and irrigation on comparative retention-cooling performance

We find that the percentage coverage of the global landmass with modelled retention performance (defined as mean AET/P) above 0.5 is 44, 66 and 82% for extensive (depth h = 50 mm), intensive (h = 150 mm) and deep (h = 1 000 mm) substrates respectively (Figure S6-S8). The respective percentage coverage for the cooling potential of (defined as mean AET/PET) above 0.5, is 43, 57 and 66% (Figure S6-S8). Budyko curves (Eq 10) and their equivalent cooling potential curves describe well the upper envelopes for the simulated range of substrate/rooting depths for the GSOD cities (Figure S9). However, deviations below these envelopes occur increasingly for higher coefficients of variation in precipitation; the same effect is also seen within the mean across all GRUMP urban areas (Figure S9). This is intuitive hydrologically, since larger or more intense rainfall events can more easily overcome antecedent soil moisture deficits leading to increased drainage and hence lower retention. Since lower retention leads to lower AET, a similar, although less pronounced, effect is also seen in the cooling potential curves. These effects are stronger the thinner the substrate/rooting depth becomes. Thus while retention shows a strong positive trend with aridity (defined as PET/P) (Figure 1A), the cooling potential shows the opposite trend (Figure 1D), and a consistent inverse relationship between retention and cooling potential is seen across different substrate/rooting depths (Figure 2B, Figure 3A).

The retention-cooling relationship can be clearly visualized in the latitudinal summaries (Figure 2B) with the steepest variations occurring across the tropics, home to nearly half of the global population[23]. For intensive urban greening, over two-thirds of the landmass (and GRUMP cities) fail to achieve simultaneous retention and cooling potential performance above 0.5. However, there are some parts of the world, most notably western equatorial Africa and southwest China, in which both cooling and retention may perform well. Such locations are characterized by energy limited (i.e. where energy rather than water is the limiting factor on rates of evapotranspiration), high humidity, conditions with associated relatively low coefficients of variation in daily precipitation (Figure 2D). Conversely, poorer performance in both metrics (<0.5) is seen in certain locations (e.g. northern India, northern Australia and western North America) associated with moderate (e.g. sub-humid to humid) aridity conditions. This trade-off between retention and cooling potential is more pronounced for thinner substrates but when irrigation is included, the strength of the trade-off between retention and cooling lessens substantially (Figure 3).
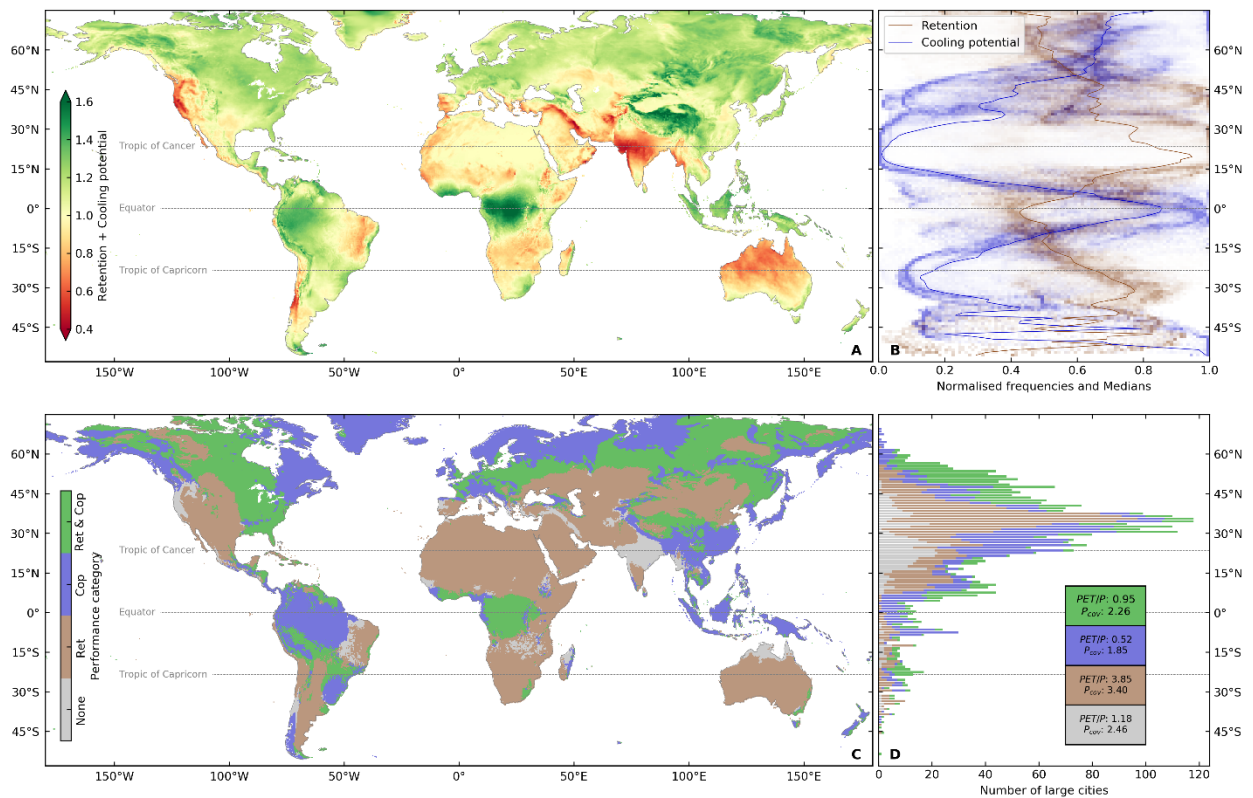

Figure 2. Global trade-offs between mean retention and cooling potential. (A) Global map of the sum of mean retention and cooling potential metrics. (B) Latitudinal summaries of mean retention and cooling potential. Shading maps the binned frequencies normalized for 1° latitude bands. Solid lines are medians across the latitudes. (C) Categorized performance of mean retention only >0.5 (Ret), mean cooling potential only >0.5 (Cop) mean retention and mean cooling potential both >0.5 (Ret & Cop) or neither mean retention or mean cooling potential >0.5 (None). (D) Latitudinal summaries by categories defined in (C) for large cities (defined as having population > 100 000 in the year 2000 CE). Inset indicates the median value of PET/P and coefficient of variation in daily precipitation (Pcov) for each mapped category. All results shown are for intensive substrates (h = 150 mm).

5

When irrigation is applied as a proportion of PET on days with no rain, no change is seen in mean retention values as calculated using Eq. 8. This is as expected since irrigation is always supplied at a rate less than the PET demand and thus AET is affected, but not drainage rates. However, very strong increases in cooling potential occur as a result of the enhanced AET. This is most pronounced in regions of higher aridity (Figure S10) where cooling potential increases of nearly 0.5 can be seen, with this effect being greater the higher the rate of applied irrigation. This suggests that irrigation may be an effective means of substantially increasing the potential cooling impacts of urban greening in areas where retention is already high, without negatively impacting the retention performance (Figure 3A). In this way the magnitude of the retention-cooling trade-off has the potential to be substantially reduced. In contrast, areas with low retention tend to be found in energy-limited environments where potential cooling may be substantial. In such locations, in order to increase retention while maintaining the high rates of cooling potential, the best option would rather be to increase the thickness, or other equivalent changes to the substrate water retention capacity, of urban greening substrates.
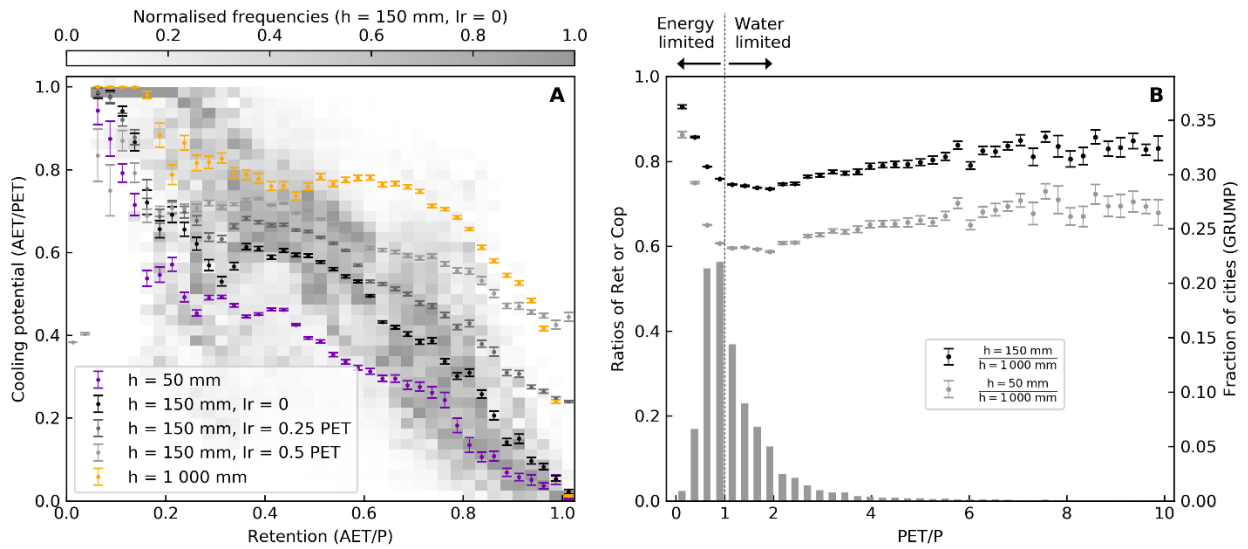

Figure 3. Variation in performance of different implementations of urban greening (A) Trade-offs between retention and cooling potential for different substrate thicknesses (h) and irrigation (Ir) applications. Points are means +/- SEM, shadings represent the binned and normalized frequency values for the intensive unirrigated substrate. (B) Histogram of global cities binned by PET/P alongside the fraction of retention or cooling potential offered by intensive substrate (h = 150 mm) and extensive substrate (h = 50 mm) as a fraction of the deep substrate (h = 1000 mm). The ratio of retention and cooling potential metrics is identical as both are equivalent to the ratio of AET between the respective substrate types. Values plotted as means +/- SEM.

For intensive or extensive urban greening, the minima of the retention performance or cooling potential plotted as a fraction of the deeper substrate simulations is close to the peak in the global city frequency histogram. This occurs around PET/P = 1, at the transition from energy limited to water limited hydrological conditions (Figure 3B). This indicates that, in average terms, strategies for urban development and renewal which create green spaces with deeply rooted vegetation offer the most potential cooling or retention as might be expected. However, extensive green substrates with just 5% (i.e. 50 mm) of the thickness of the deeper substrate may already offer around 60-90% of the possible cooling or retention gains. This figure is around 75-90% for intensive green substrates (15% of the deep substrate). Hence a combination of such urban renewal measures may be effective in mitigating the UHI effect, or

the flooding and altered hydro-ecological aspects of the USS, where greening large areas of urban spaces is possible.

Discussion

Various climate metrics are available from which to potentially test the degree of climatic control on urban greening performance. With respect to hydrological efficacy, previous work indicates that the Köppen-Geiger climate classification is a poor diagnostic indicator, at least for retention of green roofs[24]. In contrast, our results show that aridity (i.e. PET/P, or its inverse the aridity index: P/PET) is a robust indicator of the relative performance of a given urban greening intervention since it encapsulates the water or energy limiting nature of the prevailing climate, which ultimately controls the mean retention characteristics. From a thermal perspective, UHIs are often compared against precipitation as the dominant climate determinant. For example, it has been proposed recently that solutions for UHI focused on increasing vegetation cover or albedo are more likely to be efficient in "dry regions" but that other options may be required for "tropical cities"[7]. Again, here we show that aridity (PET/P) may be a more useful integrative explanatory variable than precipitation alone. Thus, while the cooling potential may indeed be bounded in some water limited tropical cities, many highly populated parts of the tropics are energy limited with high cooling potential (Figure 1, S6-7). As such, cooling via increased greening may be a viable policy option unless it becomes undesirable from a comfort perspective due to highly elevated humidity[25].

Our results also lead to the important practical implication that irrigation in more arid locations can improve the relative potential cooling performance while also maintaining substantial retention performance (Figure 3, Figure S10). However, since groundwater is the most widely available source of persistent fresh water in dryland environments[26], the water sustainability of such schemes must be considered[27] in an integrated way alongside urban development and renewal measures. One way of achieving this may be through the re-cycling of 'grey' wastewater[28]. It should also be noted that irrigation cannot add additional cooling gains in energy limited environments.

While temperate and cold climates may have less need for cooling in general terms, the increased number of droughts and heat waves is still a major concern as the climate changes[25,29]. Although there is some evidence that global warming may have complex impacts on UHI effects[30], one of the most definitive and detectable hydrological changes of global warming is the increase of precipitation intensity[31]. In this context, our results indicate that if the precipitation coefficient of variation becomes increasingly variable the hydrological and thermal performance of urban greening interventions would both diminish. Further, this effect would be more pronounced for thinner, extensive green roofs than for thicker and more deeply vegetated surfaces.

Owing to increasing population pressures and existing climate risks, urban areas play a critical role in the mitigation and adaptation to climate change; in terms of driving emissions and providing testbeds for the implementation of climate adaptation technologies and infrastructure[32]. Urban greening strategies have previously been associated with a wide range of potential environmental, economic and social ecosystem services[12,16] and while our results agree that they may be effective in contributing to urban development and renewal, they are not a panacea. For example, despite potentially being able to reduce the intensity of the urban stream syndrome (USS) through their favorable effects on stream hydrology, green roofs potentially exacerbate the USS through pollution[33,34]. Hence, while the trade-offs we focus on

here between retention and cooling may be important but manageable aspects of sustainable urban development and renewal programs, other environmental trade-offs need to be considered on a case-by-case basis.

While our results show that the ability of urban greening to simultaneously mitigate local flooding or excess heat will depend strongly on the ambient local climate and substrate thickness of urban development and renewal interventions, the precise detail of a given cityscape may add complexities not captured in our coarse-scale global analysis, e.g. due to variations in city morphology and anthropogenic heat contributions. However, since the necessary high-resolution data and modelling are not readily available for most cities around the world, our framework can provide a first-order guideline to inform generalized or large-scale strategies for urban development and renewal until more local data or models are available.

Methods

Global gridded data processing, modelling, and analysis

Global coverage of physically consistent weather variables used for modelling the hydrological and thermal performance of urban greening was obtained from the fifth generation European Medium Weather Forecast (ECMWF) atmospheric reanalysis, ERA5[35]. ERA5 outputs hourly forecast and analysis fields on a horizontal resolution of 31 km on 137 vertical levels (surface to 0.01 hPa)[17].

To estimate the potential evaporative water loss, we used the reference evapotranspiration (PET) as defined by Eq. 6 of the Food and Agriculture Organization (FAO) of the United Nations' Irrigation and Drainage Paper No 56 (ref[36]). This formula, based on the Penman-Monteith method, is adapted to be representative for a hypothetical crop surface with assumed height of 0.12 m, surface resistance of 70 s m^{-1}, and an albedo of 0.23 as follows:

$$\text{PET} = \frac{0.408\Delta(R_n - G) + \gamma\frac{900}{T+273}u_2(e_s - e_a)}{\Delta + \gamma(1 + 0.34u_2)} \qquad (Eq\ 1)$$

Estimates were calculated using ERA5 output (Table 1) for 2000-2017. Hourly re-analysis variables, downloaded with a 0.25° spatial resolution, were subsequently aggregated/averaged (as appropriate), to give a daily time step required for the hydrological modelling.

*Table S 1. **PET input variables as estimated from ERA5 variables.***

Input variable	FAO56 definition	Estimation
R_n	Net radiation at the crop surface [MJ m^{-2} day^{-1}]	Derived from ERA5 surface net solar/thermal radiation
G	Soil heat flux density [MJ m^{-2} day^{-1}]	Following Eq 42 in ref[36] $G_{day} \approx$ zero
T	Mean daily air temperature at 2 m height [°C]	ERA5 2 m temperature
u_2	Wind speed at 2 m height [m s^{-1}]	Derived from ERA5 10 m u and v components and downscaled using Eq 47 in ref[36]
e_s	Saturation vapor pressure [kPa]	Estimated from ERA5 2 m temperature using Eq 11 in ref[36]
e_a	Actual vapor pressure [kPa]	Estimated from ERA5 2 m dewpoint temperature using Eq 14 in ref[36]
γ	Psychrometric constant [kPa °C[-1]]	Estimated using Eq. 7 and 8 from ref[36] using ERA5 geopotential to derive elevation above sea level
Δ	Slope vapor pressure curve [kPa °C[-1]]	Estimated from ERA5 2m temperature using Eq 13 from ref[36]

Global cities data processing, modelling, and analysis

To model the hydrological and thermal performance of urban greening using representative field datasets, urban areas with appropriate long-term Global Surface Summary of the Day[19] precipitation measurements were identified from those cross-checked for quality

and applicability to large urban areas for hydrological application by Mishra et al. (ref[37]). The datasets for 214 stations were downloaded from the National Oceanic and Atmospheric Administration (NOAA), unpacked and assembled as continuous daily time series. Missing values were flagged, and units were converted to International System of Units (SI) before further processing. Precipitation gaps smaller than 370 days were infilled using data from the Global Precipitation Climatology Centre[38] from the longitude/latitude cell within which the station is located. This resulted in a median and maximum number of infilled days of 1.57 and 1095 respectively. Data for 175 cities having at least 15 years duration to overlap with the ERA5 data (for years 2000 to 2015) were retained and used as input files for simulating the water retention and cooling performance of urban greening as described below.

Urban greening model description, evaluation, and global application

Soil moisture balance models (SMBMs) are standard tools in hydrology for simulating evapotranspiration and drainage, for example in the context of estimating crop irrigation water requirements[36], evaluating moisture deficits in soils[39,40], and estimating deep drainage (i.e. groundwater recharge)[26]. More recently SMBMs have also been successfully evaluated for quantifying the water balance of engineered green substrates as specifically applied to urban greening measures such as green roofs across a range of climates[24,41-43]. As such, they are a well understood and demonstrably robust tool for simulating the hydrology of a wide variety of planted green urban surfaces under diverse climatic settings with or without irrigation. However, existing modelling studies have so far not dealt with the issue of equifinality[44], in which there may be multiple parameter sets providing equally good or acceptable model outputs. This is important to consider in a study of this kind to ensure the choice of model parameters applied at the global scale does not bias the overall results. Hence, here we first developed a standard but parsimonious SMBM. We then evaluated it using field data across a range of climates with a Monte-Carlo based multi-parameter uncertainty analysis to estimate the likely error involved in the parameter choices, before applying it globally.

Model Description

The total available water (TAW) is defined as:

$$TAW = h(FC - WP) \tag{Eq 2}$$

where z is the effective depth of rooting (m), FC is the field capacity (m^3/m^3) and WP is the wilting point (m^3/m^3). Since TAW is proportional to both h and $FC\text{-}WP$, and thus influence the model sensitivity in a correlated way, only $FC\text{-}WP$ was varied in the parameter sensitivity analysis outlined below while we fixed the effective rooting depth as equal to substrate depth. The readily available water (RAW) is a fixed proportion of the TAW:

$$RAW = p_c TAW \tag{Eq 3}$$

where p_c is a constant (dimensionless). The model requires forcing time series of reference crop evapotranspiration (PET) and precipitation (P), and optionally also irrigation (Ir). Overland flow has been assumed to be zero with all rainfall becoming evaporation or infiltration as appropriate to well-drained engineered surfaces. The model follows the FAO56 'single crop-coefficient' approach[36] whereby the effect of both crop transpiration and soil evaporation are integrated into a combined crop coefficient (k_c) to estimate potential evapotranspiration (PET) demand from PET as follows:

$$PET_c = k_c PET \tag{Eq 4}$$

Vegetative stress and limits to soil evaporation under dry soil conditions are controlled using a stress co-efficient (K_s, dimensionless) as follows:

$$K_s(t) = \frac{TAW - SMD(t)}{TAW - RAW} \tag{Eq 5}$$

where t is time, SMD is the soil moisture deficit (m). If $P_t + Ir_t < \text{PET}_{c,t}$, all the rainfall and irrigation becomes actual evapotranspiration (AET_t, m) plus a further amount taken from the soil store equal to the remaining evaporative demand modified by the stress co-efficient as follows:

$$AET_t = K_{s,t} PET_{c,t} \tag{Eq 6}$$

If $P_t + Ir_t > \text{PET}_{c,t}$, then the excess precipitation reduces the SMD but if the SMD reaches zero then any further moisture excess becomes drainage (D_t) (this is equivalent to what is termed 'runoff' in some green roof modelling studies). The overall mass balance equation that controls the state variable SMD is as follows:

$$SMD_{t+1} = SMD_t - (P_t + Ir_t) + AET_t + D_t \tag{Eq 7}$$

Model Uncertainty Analysis

As discussed above, for the global application of the SMBM it is important to quantify the impact of equifinality on the overall uncertainty of the SMBMs for any particular parameter combination. To do this we took advantage of data from a recent unique field study in which climate and drainage data were collected for identical experimental green roofs in three contrasting Canadian climates[10]. The sites have long-term aridity index (P/PET) values of 0.64 (Calgary, Alberta), 1.35 (London, Ontario) and 2.34 (Halifax, Nova Scotia), representing the aridity range of more than 70% of global cities (using climate data from ref[45] and the GRUMP global cities database[18]). On-site climate observations were used to calculate a daily time series of PET using the FAO Penman-Monteith equations (see ERA5 section above) and precipitation to drive the models, and the modelled drainage was compared to observed values.

To assess the combined parameter and data input uncertainty, 10 000 Monte Carlo Experiments (MCEs) were run using the same parameters for all roofs for each simulation. Forcing P and PET were run with added random noise at the 10% level to account for instrument uncertainties, and all parameters were randomly sampled from 'a priori' parameter ranges as follows: 0 to 0.3 for FC-WP, 0.5 to 1.5 for k_c and 0.3 to 0.7 for p_c. The thickness parameter h was set to the known depth of the roof substrate (0.15 m).

Any individual model was accepted as behavioral if its Nash-Sutcliffe Efficiency (NSE) was > 0.7 with the additional criterion that the mean NSE across all sites was > 0.8. A linear regression model was also fitted 'post-hoc' to give an additional evaluation metric to compare the magnitudes of observed and simulated drainage events via the R^2 value. Time series and cumulative time series are shown in Figure S1. Runs with acceptable NSE values also all have R^2 values above 0.84 (Figure S2). This is indicative of excellent model performance both in terms of timing of drainage and cumulative drainage, and therefore also of mean retention and AET.

Finally, to assess the overall uncertainty of a particular choice of parameters for the subsequent global models, the behavioral parameter sets from the MCEs were simulated for all the GSOD city data locations, forced using GSOD precipitation and ERA PET. The results indicate that the relative standard error is less than approximately 1% across all behavioral parameter sets for PET/P values from 0 to 8 i.e. ranging from hyper-humid to arid climates. This indicates that application of our model to the range of global climates is very insensitive to a choice of particular parameters from the behavioral set. As a result we decided to apply our best 'a priori' estimate of parameters for a typical green roof for the global simulations as follows: $k_c = 1.0$, FC-WP = 0.12 (equivalent to a sand-loam substrate), and $p_c = 0.5$. This set of behavioral parameters works very well for the green roof evaluation ($R^2 > 0.85$) but also has

11

the added advantage of being an appropriate choice, in combination with a larger value of substrate depth (*h*), for the simulation of grassed surfaces which tend to dominate in urban parks[36].

Global Application

For the global calculations, three substrate thickness scenarios were assigned of 150 mm ('intensive' substrate), 50 mm ('extensive' substrate) and 1 000 mm ('deep' substrate emulating, for example, a ground level park or recreational area).

These scenarios were run globally using ERA5 PET and P values on a 0.25° grid for the period 2000-2017 on a daily timestep. Whilst this approach allows a globally consistent estimate of PET, we acknowledge that underlying assumptions in the formulation of PET are partly violated; i.e., the assumption that input weather data are representative of surface weather conditions above a well-watered crop surface, which ideally extend at least 100 m in each direction of the weather station[46]. In using re-analysis, we also violate the assumed scale (point to areal estimate) and surface homogeneity. Because spatial disaggregation typically implies an amplification of uncertainties[47], we can assume that in using ERA5 over point measurements, we are reducing representation of uncertainty in the estimates as we are effectively smoothing spatial variability in using coarser resolution data.

In addition to the simulations using only natural precipitation, we have run two global models which assume the addition of irrigation, to test its impact on the retention and cooling potential performance. For these runs we used the intensive substrate model (*h* = 150 mm) as a baseline and applied additional water only on days of no rainfall, as a rate equal to either 25% or 50% of the PET for that day.

Modelled outputs were extracted from the global ERA5 runs to form a subset at the locations of 31500 urban areas worldwide[18]. In order to test the sensitivity of the results to the use of gridded (ERA5) versus 'point' (weather station observations) precipitation data[48], we also ran identical models for the time period 2000-2015 using both gridded and site observation precipitation data for the GSOD locations (see above). Implicit in our modelling is that local vegetation types would be chosen to account for the local climate conditions, but for purposes of global comparisons, we assume a single *kc* everywhere.

Metrics and empirical models of hydrological and thermal performance

Hydrological Retention:

As is conventional in the urban greening literature, hydrological retention (Ret) was calculated as the difference in the incident precipitation and subsequent drainage over a given period, normalized by the precipitation over the same period as follows:

$$Ret = \frac{\bar{P} - \bar{D}}{\bar{P}} \qquad \text{(Eq 8)}$$

Over the long timescales simulated this can also be expressed as:

$$Ret = \frac{\overline{AET}}{\bar{P}} \qquad \text{(Eq 9)}$$

The retention is expressed as a proportion of the incident precipitation, so we are not making any assumptions about the percentage spatial coverage in a particular location. Rather, the only assumption implicit in using this metric is that the total amount of retention that is possible will scale linearly with changes in the proportion of a certain type of urban cover. Hence this dimensionless retention metric can be used to represent the relative retention performance of (1) different urban greening interventions at any given location, or (2) the same urban greening intervention at different locations.

Cooling potential:

It has recently been demonstrated that the prevailing climate is the main control on the magnitude of the urban heat island effects globally[6,7] primarily due to the dominant effect of changing landcover on the rates of evaporative cooling. Hence, in non-irrigated situations we would expect that the observed urban heat island (UHI) effect on surface temperatures would be approximately mitigated by re-establishing AET of native vegetation. This finding led us to seek a parsimonious heuristic metric of relative cooling potential (CP) which could be used for comparing the relative performance of a particular urban greening intervention between different locations globally. Initial exploration demonstrated that a simple scaling of AET (for which we used global AET data from GLEAM[49]), leads to too linear a relationship with climate as compared to existing UHI data. However, we found that also normalizing by the potential evapotranspiration rate leads to a very strong correspondence with observations (Figure S5). The Budyko framework can conveniently be used to describe this scaling as follows.

The commonly employed Turc (1954) formulation[50] which requires one parameter (γ) to control the Budyko curve as follows:

$$\frac{\overline{AET}}{\bar{P}} = \emptyset(1 + \emptyset^\gamma)^{-\frac{1}{\gamma}} \qquad \text{(Eq 10)}$$

where $\emptyset = \frac{\overline{PET}}{\bar{P}}$.

Considering the difference between rural and urban Budyko curves (parameters γ_r and γ_u respectively) for any climate, adding an empirical scaling factor (f, $(°C)^{-1}$)), and re-arranging, we can write:

$$\Delta T_s \equiv \frac{(1 + \emptyset^{\gamma r})^{-\frac{1}{\gamma r}} - (1 + \emptyset^{\gamma u})^{-\frac{1}{\gamma u}}}{f} \equiv \frac{\Delta\left(\frac{\overline{AET}}{\bar{P}}\right)}{\left(\frac{\overline{PET}}{\bar{P}}\right)f} \equiv \frac{\Delta\overline{AET}}{\overline{PET}.f} \qquad \text{(Eq 11)}$$

Where ΔT_s is the potential urban heat island effect (°C), and thus the maximum potential cooling afforded by complete urban 'renewal' as an UHI mitigation measure. This grows as the difference between the Budyko curves, and thus the difference in native and urban evapotranspiration ($\Delta\overline{AET}$), grows. The divisor empirically accounts for other controls on the UHI (e.g. predominantly changes in convective efficiency[7]) as well as variation of temperature sensitivities to changes in energy forcing at the land surface.

We demonstrate the effective performance of this empirical model by assuming a rural global Budyko value in the range 1.4 to 2.6 (ref[51]) and factor this by a mean estimate of the global green urban proportion of 15% (ref[7]) to yield a range of urban Budyko values. We then ran 1000 Monte Carlo realizations for uniform random combinations across the range these urban and rural Budyko curves while fitting models using a single global value of the unconstrained empirical parameter f. We find this heuristic model can explain 68-73% of the variance in the global mean UHI data[21] when plotted against aridity (Figure S5A). This is further evaluated by showing that the model explains >70% of the variance in the global UHI data when plotted against precipitation (Figure S5B). We note this gives similar performance to a more complex coarse-grained UHI model[7] when compared to the equivalent, but more limited, global UHI dataset that was used in that study[20] (also plotted for comparison purposes in Figure S5).

To use this result for the purpose of approximating the relative cooling effect as a comparator from one location to another, or between different substrate choices at the same location, we can discard the constant f and define a dimensionless cooling potential as equal to:

$$CP = \frac{\overline{AET}}{\overline{PET}}$$
(Eq 12)

Given the demonstrated insensitivity of changes in ΔT_s to changes in urban green cover (gc,u) for any given mean precipitation[7] this metric can be considered applicable for any given change in urban green cover i.e. the reduction in the UHI can be expected to occur linearly with increasing urban green cover in a given climate.

The cooling potential metric we propose is therefore a practical approximation of the relative potential thermal performance of (a) different urban greening interventions at any given location, or (b) the same urban greening intervention at different locations. The dimensionless nature of cooling potential also makes it readily applicable for making comparisons to the dimensionless retention metric enabling us to straightforwardly combine and compare the metrics to consider the trade-offs globally using the comparative performance of each (e.g. Figure 2).

Comparison of re-analysis and point data

Using gridded ERA5 precipitation data yields a bias of 3% ($R^2 = 0.87$) in cooling potential and 10% ($R^2 = 0.62$) in retention versus simulations using 'point' GSOD city precipitation data. This is expected due to a fundamental scale discrepancy between the modelled areal estimate and point measurements[48], and influences of any structural or parametric inadequacies in the model used to generate the re-analysis. Different regional assessments of ERA5 precipitation suggest performance varies geographically and depending on the metric of interest. For example, ERA5 provides realistic estimates of water and energy budgets for the Canadian prairies[52], and is able to reproduce spatial precipitation distribution and light to medium quantities for Austria, but it systematically overestimates on monthly time scales[53]. For Bangladesh, compared to other gridded rainfall products, ERA5 shows good performance for rainfall detection metrics with low false alarm ratio metrics for the higher quantiles[54]. However, when station networks are sparse, re-analysis datasets can provide meaningful and spatiotemporally complete input datasets to hydrological modelling[55].

The strong correlations for outputs based on ERA5 and point data gives us confidence to draw conclusions about the urban greening metrics (retention and cooling potential) and their climate relationships. Furthermore, the GSOD cities represent a subset that is consistent within the global range in the Budyko parameter space (Figure 1C) including for potential cooling (Figure 1F). Hence, for this study, we consider that ERA5 provides a robust and physically consistent dataset to derive global patterns on retention and cooling potential.

Author contributions: Conceptualization: Conceived by MOC and refined by all authors. Methodology: MOC, ME, GCR. Analysis: MOC, GCR, ME, DO'C. Visualization: GCR, MOC. Writing: MOC with input from all authors.

Competing interests: Authors declare no competing interests.

Materials & Correspondence: to Mark Cuthbert cuthbertm2@cardiff.ac.uk

Data availability: All data and code used in the main text or the supplementary materials is available online from https://figshare.com/authors/Mark_Cuthbert/3847054 or on request from the corresponding author.

References

1   U. Nations. *2018 revision of world urbanization prospects* (United Nations New York, 2018).

2   Bowler, D. E., Buyung-Ali, L., Knight, T. M. & Pullin, A. S. Urban greening to cool towns and cities: A systematic review of the empirical evidence. *Landscape and urban planning* **97**, 147-155 (2010).

3   Kundzewicz, Z. W. *et al.* Flood risk and climate change: global and regional perspectives. *Hydrological Sciences Journal* **59**, 1-28 (2014).

4   Mora, C. *et al.* Global risk of deadly heat. *Nature Climate Change* **7**, 501-506 (2017).

5   Jim, C. Y. Sustainable urban greening strategies for compact cities in developing and developed economies. *Urban Ecosystems* **16**, 741-761 (2013).

6   Li, D. *et al.* Urban heat island: Aerodynamics or imperviousness? *Science Advances* **5**, eaau4299 (2019).

7   Manoli, G. *et al.* Magnitude of urban heat islands largely explained by climate and population. *Nature* **573**, 55-60 (2019).

8   Larsen, T. A., Hoffmann, S., Lüthi, C., Truffer, B. & Maurer, M. Emerging solutions to the water challenges of an urbanizing world. *Science* **352**, 928-933 (2016).

9   Zhao, L., Lee, X., Smith, R. B. & Oleson, K. Strong contributions of local background climate to urban heat islands. *Nature* **511**, 216-219 (2014).

10   Sims, A. W. *et al.* Retention performance of green roofs in three different climate regions. *Journal of Hydrology* **542**, 115-124 (2016).

11   Booth, D. B., Roy, A. H., Smith, B. & Capps, K. A. Global perspectives on the urban stream syndrome. *Freshwater Science* **35**, 412-420 (2016).

12   Tabatabaee, S., Mahdiyar, A., Durdyev, S., Mohandes, S. R. & Ismail, S. An assessment model of benefits, opportunities, costs, and risks of green roof installation: A multi criteria decision making approach. *Journal of Cleaner Production* **238**, 117956 (2019).

13   Walsh, C. J. *et al.* The urban stream syndrome: current knowledge and the search for a cure. *Journal of the North American Benthological Society* **24**, 706-723 (2005).

14   Wang, W. & Shu, J. Urban renewal can mitigate urban heat islands. *Geophysical Research Letters* **47**, e2019GL085948 (2020).

15   Grimm, N. B. *et al.* Global change and the ecology of cities. *Science* **319**, 756-760 (2008).

16   Oberndorfer, E. *et al.* Green roofs as urban ecosystems: ecological structures, functions, and services. *BioScience* **57**, 823-833 (2007).

17   Hersbach, H. *et al.* The ERA5 global reanalysis. *Quarterly Journal of the Royal Meteorological Society* (2020).

18   Center for International Earth Science Information Network - CIESIN - Columbia University, International Food Policy Research Institute - IFPRI, The World Bank, Centro Internacional de Agricultura Tropical - CIAT. (NASA Socioeconomic Data and Applications Center (SEDAC), Palisades, NY, 2011). https://doi.org/10.7927/H4GH9FVG

19.   User Engaement and Services Branch. (2020) Global Summary of the Day. https://data.nodc.noaa.gov/cgi-bin/iso?id=gov.noaa.ncdc:C00516

20   Center for International Earth Science Information Network - CIESIN - Columbia University. (NASA Socioeconomic Data and Applications Center (SEDAC), Palisades, NY, 2016). https://doi.org/10.7927/H4H70CRF

21   Chakraborty, T. & Lee, X. A simplified urban-extent algorithm to characterize surface urban heat islands on a global scale and examine vegetation control on their spatiotemporal variability. *International Journal of Applied Earth Observation and Geoinformation* **74**, 269-280 (2019).

22   Budyko, M. I., Miller, D. H. & Miller, D. H. *Climate and life*. Vol. 508 (Academic press New York, 1974).

23   State of the Tropics, *State of the Tropics 2020 Report.* (James Cook University, Townsville, Australia, 2020).

24   Hellies, M., Deidda, R. & Viola, F. Retention performances of green roofs worldwide at different time scales. *Land Degradation & Development* **29**, 1940-1952 (2018).

25   Buzan, J. R. & Huber, M. Moist heat stress on a hotter Earth. *Annual Review of Earth and Planetary Sciences* **48** (2020).

26   Cuthbert, M. O. *et al.* Observed controls on resilience of groundwater to climate variability in sub-Saharan Africa. *Nature* **572**, 230-234 (2019).

27   Gleeson, T., Cuthbert, M., Ferguson, G. & Perrone, D. Global Groundwater Sustainability, Resources, and Systems in the Anthropocene. *Annual Review of Earth and Planetary Sciences* **48** (2020).

28   Li, F., Wichmann, K. & Otterpohl, R. Review of the technological approaches for grey water treatment and reuses. *Science of the total environment* **407**, 3439-3449 (2009).

29   Huong, H. T. L. & Pathirana, A. Urbanization and climate change impacts on future urban flooding in Can Tho city, Vietnam. *Hydrology and Earth System Sciences* **17**, 379 (2013).

30   Scott, A. A., Waugh, D. W. & Zaitchik, B. F. Reduced Urban Heat Island intensity under warmer conditions. *Environmental Research Letters* **13**, 064003 (2018).

31   Wang, G. *et al.* The peak structure and future changes of the relationships between extreme precipitation and temperature. *Nature Climate Change* **7**, 268-274 (2017).

32   Bazaz, A. *et al.* Summary for urban policymakers: What the IPCC Special Report on global warming of 1.5° C means for cities. (2018).

33   Karczmarczyk, A., Baryła, A., Fronczyk, J., Bus, A. & Mosiej, J. Phosphorus and Metals Leaching from Green Roof Substrates and Aggregates Used in Their Composition. *Minerals* **10**, 112 (2020).

34   Mitchell, M., Hamilton, T., Uebel-Niemeier, C., Hopfensperger, K. & Buffam, I. Nitrogen cycling players and processes in green roof ecosystems. *Applied Soil Ecology* **132**, 114-125 (2018).

35   Service, C. C. C. ERA5: Fifth generation of ECMWF atmospheric reanalyses of the global climate. (2017).

36   Allen, R. G., Pereira, L. S., Raes, D. & Smith, M. FAO Irrigation and drainage paper No. 56. *Rome: Food and Agriculture Organization of the United Nations* **56**, e156 (1998).

37   Mishra, V., Ganguly, A. R., Nijssen, B. & Lettenmaier, D. P. Changes in observed climate extremes in global urban areas. *Environmental Research Letters* **10**, 024005 (2015).

38   Schneider, U. *et al.* GPCC full data reanalysis version 6.0 at 0.5: monthly land-surface precipitation from rain-gauges built on GTS-based and historic data. *GPCC Data Rep., doi* **10** (2011).

39   Rushton, K., Eilers, V. & Carter, R. Improved soil moisture balance methodology for recharge estimation. *Journal of Hydrology* **318**, 379-399 (2006).

40   Warter, M. M. *et al.* Onset and propagation of drought into soil moisture and vegetation responses during the 2012–2019 drought in Southern California. *Hydrology and Earth System Sciences Discussions*, 1-35 (2020).

41   Stovin, V., Poë, S. & Berretta, C. A modelling study of long term green roof retention performance. *Journal of environmental management* **131**, 206-215 (2013).

42   Talebi, A., Bagg, S., Sleep, B. E. & O'Carroll, D. M. Water retention performance of green roof technology: A comparison of canadian climates. *Ecological engineering* **126**, 1-15 (2019).

43   Viola, F., Hellies, M. & Deidda, R. Retention performance of green roofs in representative climates worldwide. *Journal of Hydrology* **553**, 763-772 (2017).

44   Beven, K. & Binley, A. The future of distributed models: model calibration and uncertainty prediction. *Hydrological processes* **6**, 279-298 (1992).

45   Knoben, W. J., Woods, R. A. & Freer, J. E. A quantitative hydrological climate classification evaluated with independent streamflow data. *Water Resources Research* **54**, 5088-5109 (2018).

46   Pereira, L. S., Allen, R. G., Smith, M. & Raes, D. Crop evapotranspiration estimation with FAO56: Past and future. *Agricultural Water Management* **147**, 4-20 (2015).

47   Raupach, M. & Finnigan, J. Scale issues in boundary-layer meteorology: Surface energy balances in heterogeneous terrain. *Hydrological Processes* **9**, 589-612 (1995).

48   Osborn, T. J. Areal and point precipitation intensity changes: Implications for the application of climate models. *Geophysical research letters* **24**, 2829-2832 (1997).

49   Martens, B. *et al.* GLEAM v3: Satellite-based land evaporation and root-zone soil moisture. *Geoscientific Model Development* **10**, 1903-1925 (2017).

50   Lhomme, J.-P. & Moussa, R. Matching the Budyko functions with the complementary evaporation relationship: consequences for the drying power of the air and the Priestley-Taylor coefficient. *Hydrology and Earth System Sciences* **20**, 4857 (2016).

51   Li, D., Pan, M., Cong, Z., Zhang, L. & Wood, E. Vegetation control on water and energy balance within the Budyko framework. *Water Resources Research* **49**, 969-976 (2013).

52   Betts, A. K., Chan, D. Z. & Desjardins, R. L. Near-surface biases in ERA5 over the Canadian Prairies. *Frontiers in Environmental Science* **7**, 129 (2019).

53   Sharifi, E., Eitzinger, J. & Dorigo, W. Performance of the State-Of-The-Art Gridded Precipitation Products over Mountainous Terrain: A Regional Study over Austria. *Remote Sensing* **11**, 2018 (2019).

54   Islam, M. A. & Cartwright, N. Evaluation of climate reanalysis and space-borne precipitation products over Bangladesh. *Hydrological Sciences Journal* **65**, 1112-1128 (2020).

55   Essou, G. R., Brissette, F. & Lucas-Picher, P. The use of reanalyses and gridded observations as weather input data for a hydrological model: Comparison of performances of simulated river flows based on the density of weather stations. *Journal of Hydrometeorology* **18**, 497-513 (2017).

Supplementary Figures for:
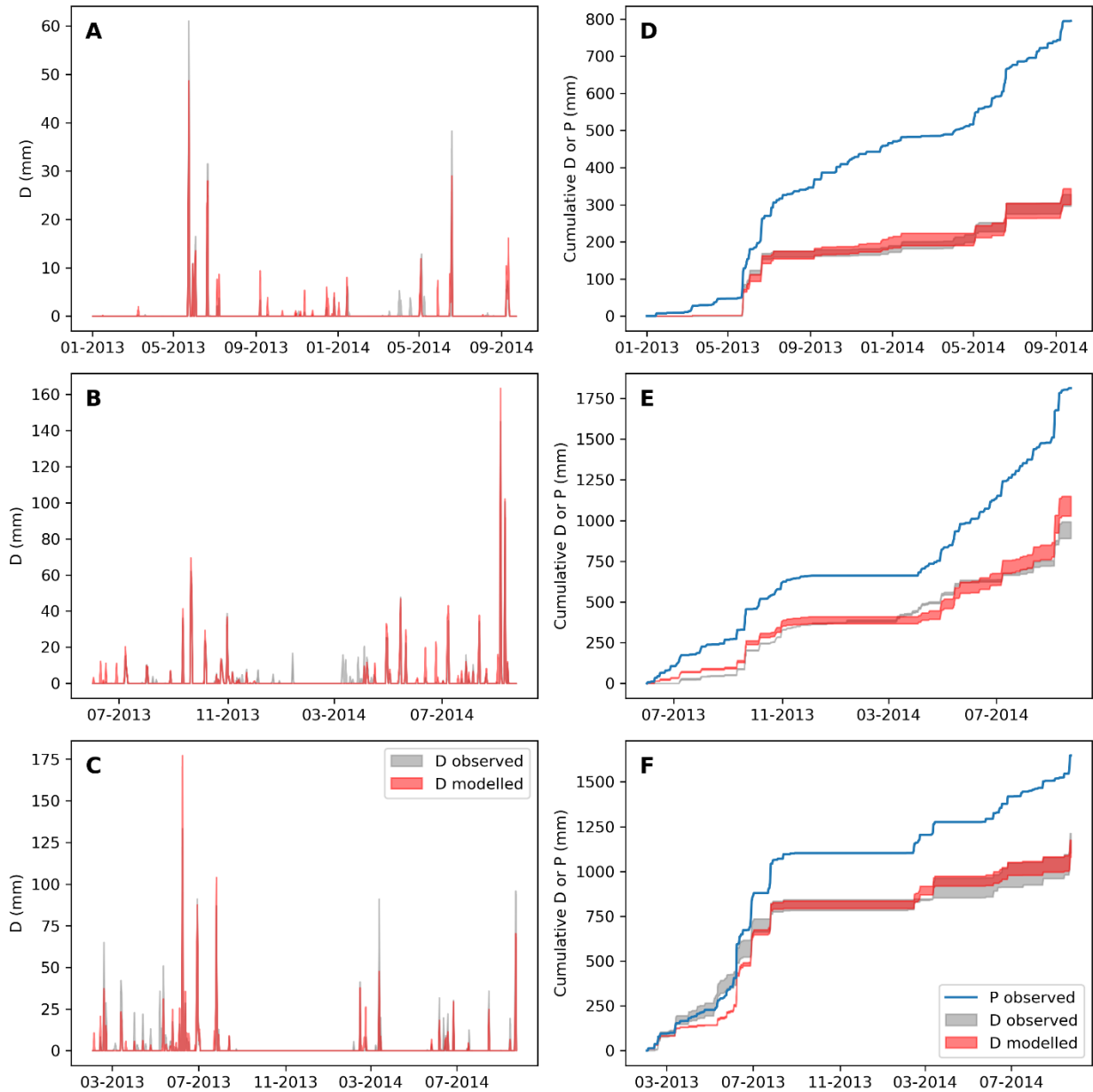
*Figure S1. Time series of modelled and observed green roof drainage (D) and cumulative precipitation (P) and drainage for behavioral simulations for 3 Canadian roofs in different climates located in (**A,D**) Halifax, (**B,E**) Calgary and (**C,F**) London.*
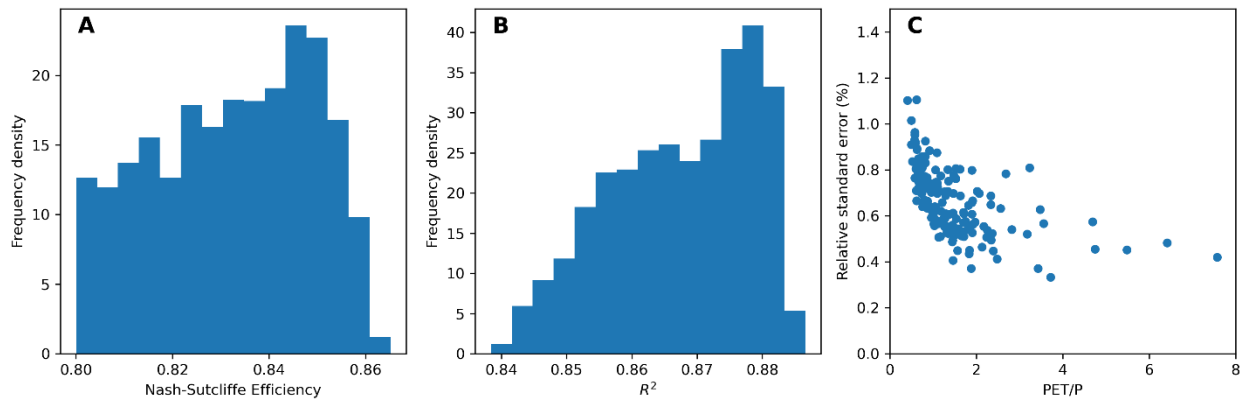
*Figure S2. Model evaluation statistics for best performing Monte-Carlo Experiments (MCEs) expressed as means for simulations of 3 Canadian roofs in different climates (**A**) Nash-Sutcliffe Efficiency in modelled versus observed drainage (**B**) Coefficient of determination in modelled versus observed drainage. (**C**) Relative standard error for the outputs of all behavioral parameter sets derived from the MCEs applied to the collated GSOD city locations, plotted against aridity.*
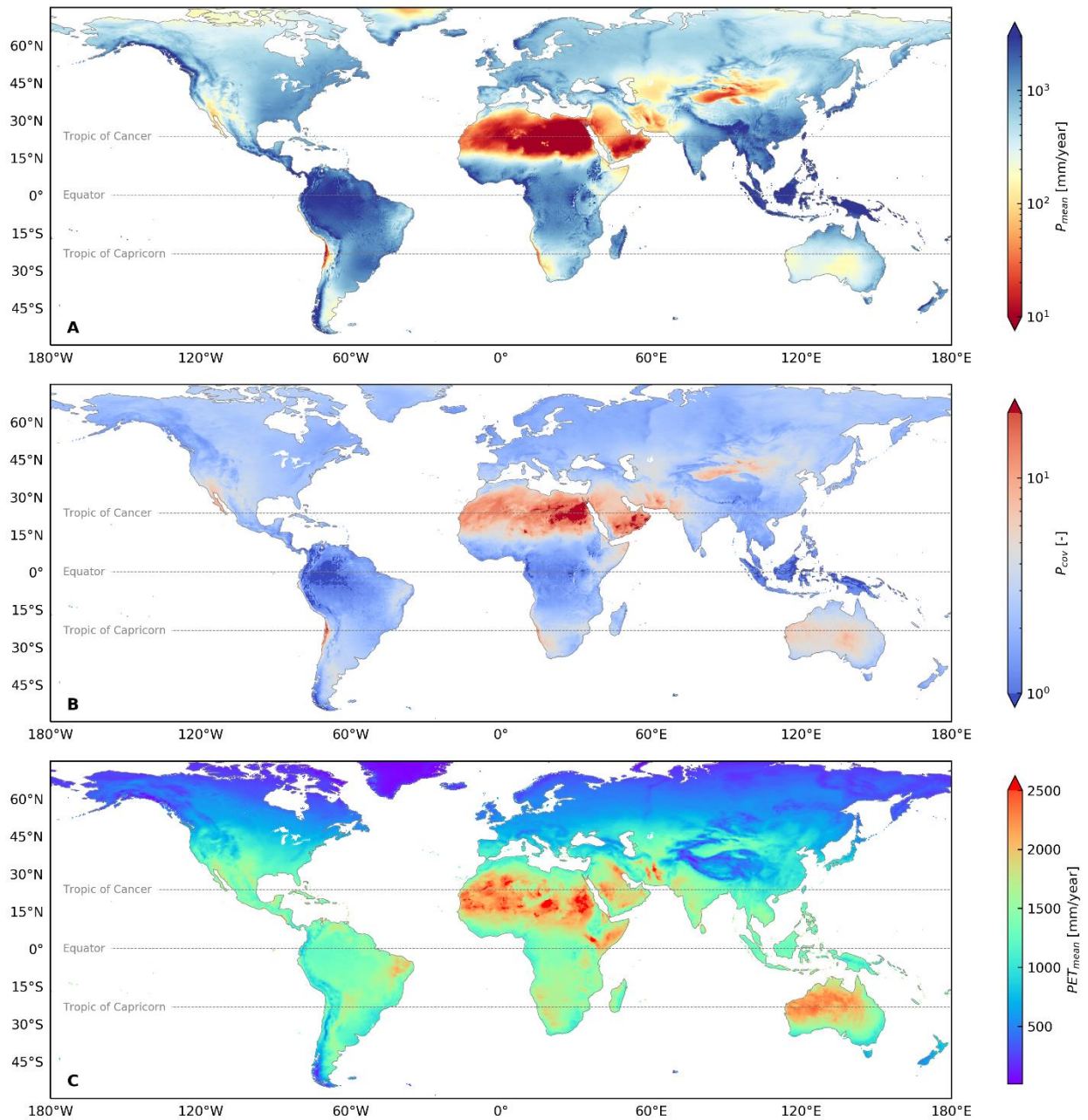
*Figure S3 Maps of ERA5 derived global climate parameters for (**A**) mean precipitation (P) (**B**) coefficient of variation in daily precipitation (P_{cov}) and (**C**) mean reference crop potential evapotranspiration (PET)*
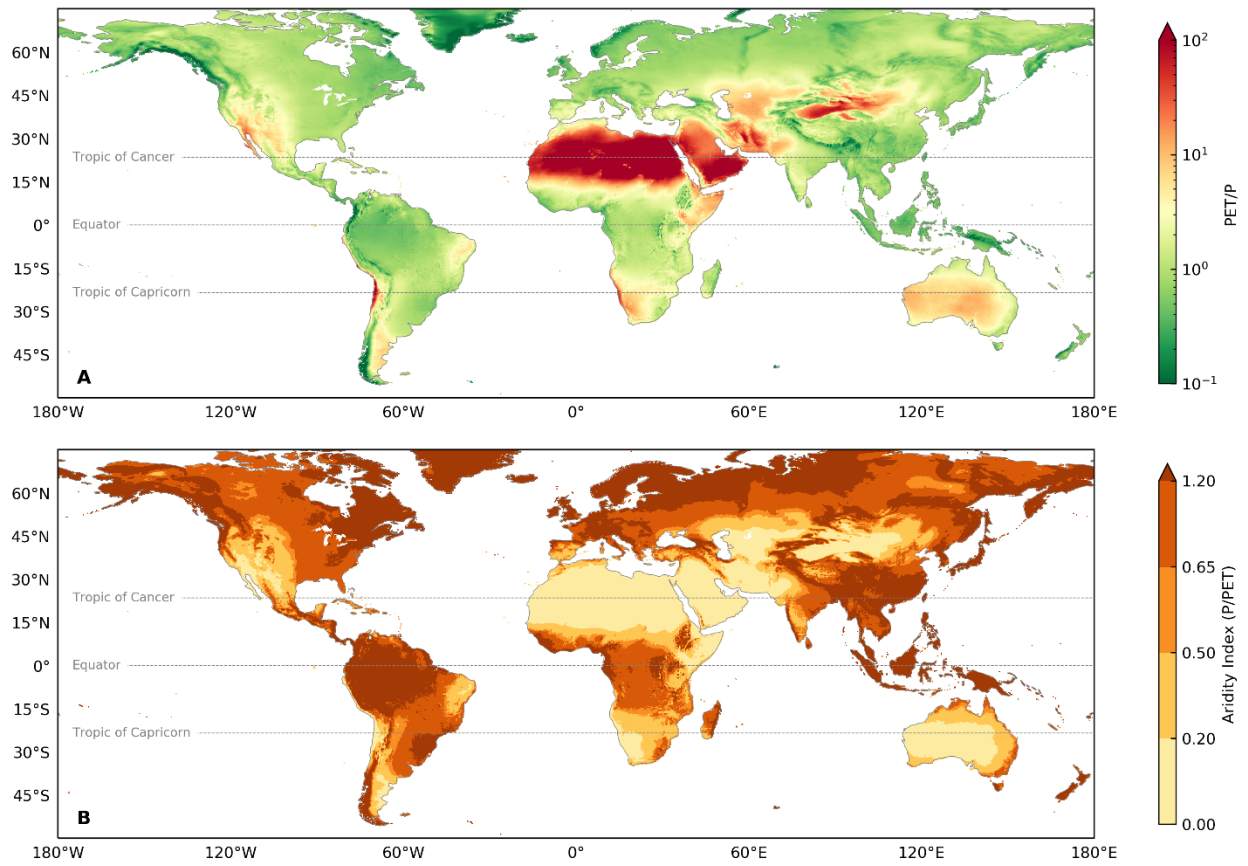
*Figure S4. Maps of ERA5 derived global climate parameters for (**A**) mean reference crop potential evapotranspiration divided by mean precipitation (**B**) Aridity Index equal to mean precipitation divided by mean reference crop potential evapotranspiration.*

.
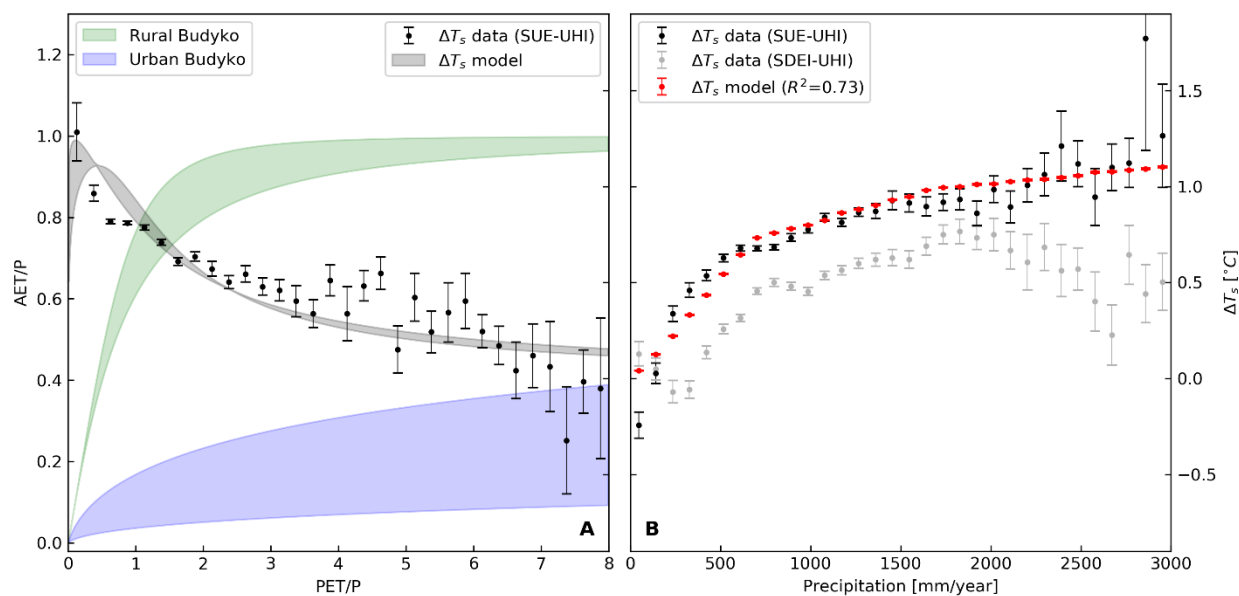
*Figure S5 (**A**) Comparison of mean urban-rural surface temperature difference (SUE-UHI[21] ΔTs) with the empirical model given by Equation 15 across a range of realistic urban-to-rural Budyko curves. (**B**) Evaluation of best model fit against Precipitation. SDEI-UHI data[20] also shown for comparison. Error bars are equal to the SEM.*
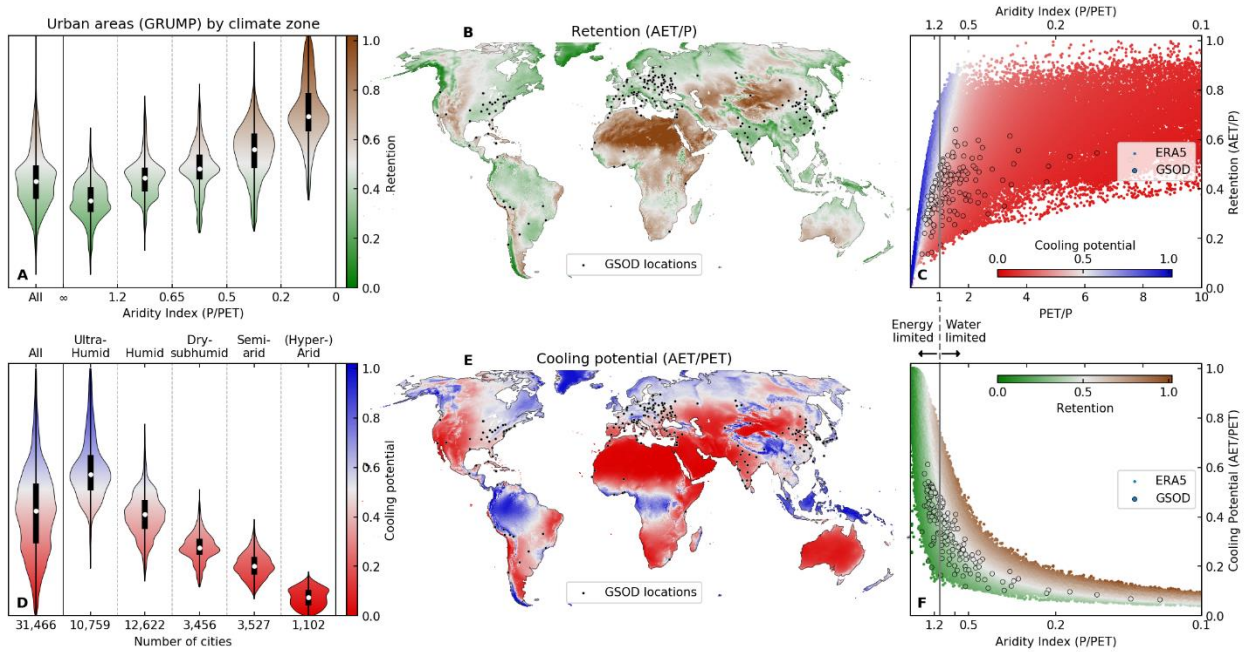
*Figure S6. Global distributions and interrelationships of ERA5 forced models using 'extensive substrate' (h = 50 mm) for: (**B, C**) Retention and (**E, F**) Cooling Potential. (**A, D**) Violin plots extracted for GRUMP urban areas only. GSOD city point-data and locations shown for reference in (**B, C**) and (**E, F**).*
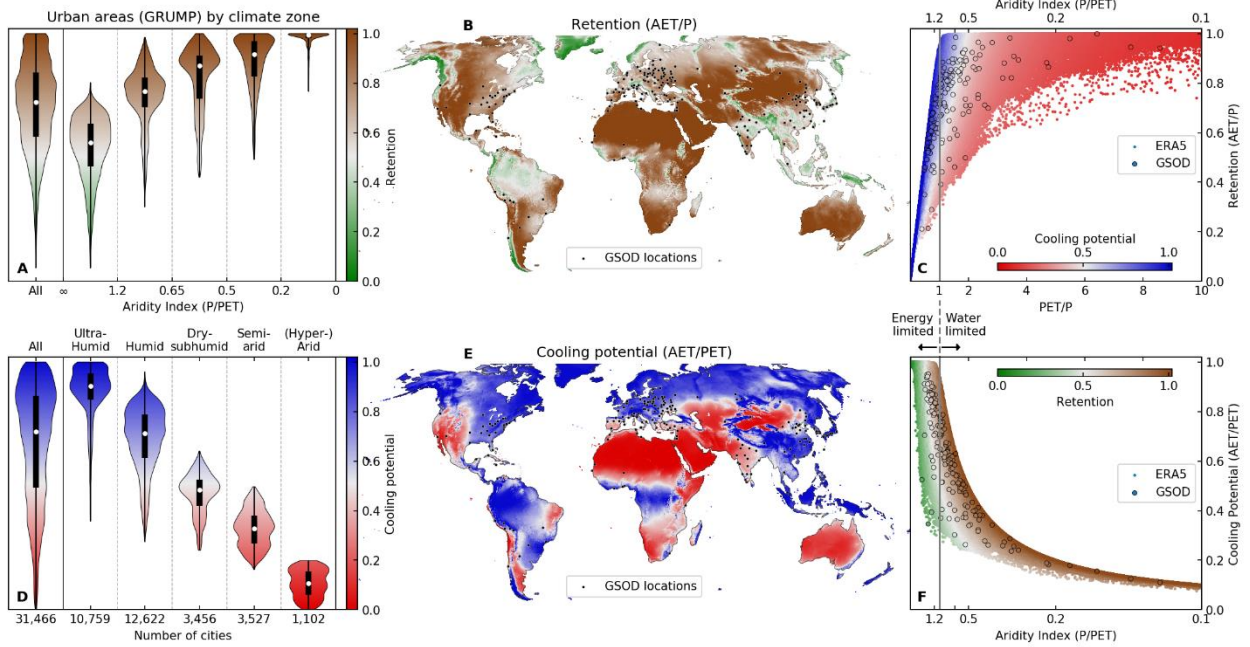
*Figure S7. Global distributions and interrelationships of ERA5 forced models using 'deep substrate' (h = 1000 mm) for: (**B,C**) Retention and (**E,F**) Cooling Potential. (**A,D**) Violin plots extracted for GRUMP urban areas only. GSOD city point-data and locations shown for reference in (**B, C**) and (**E, F**).*
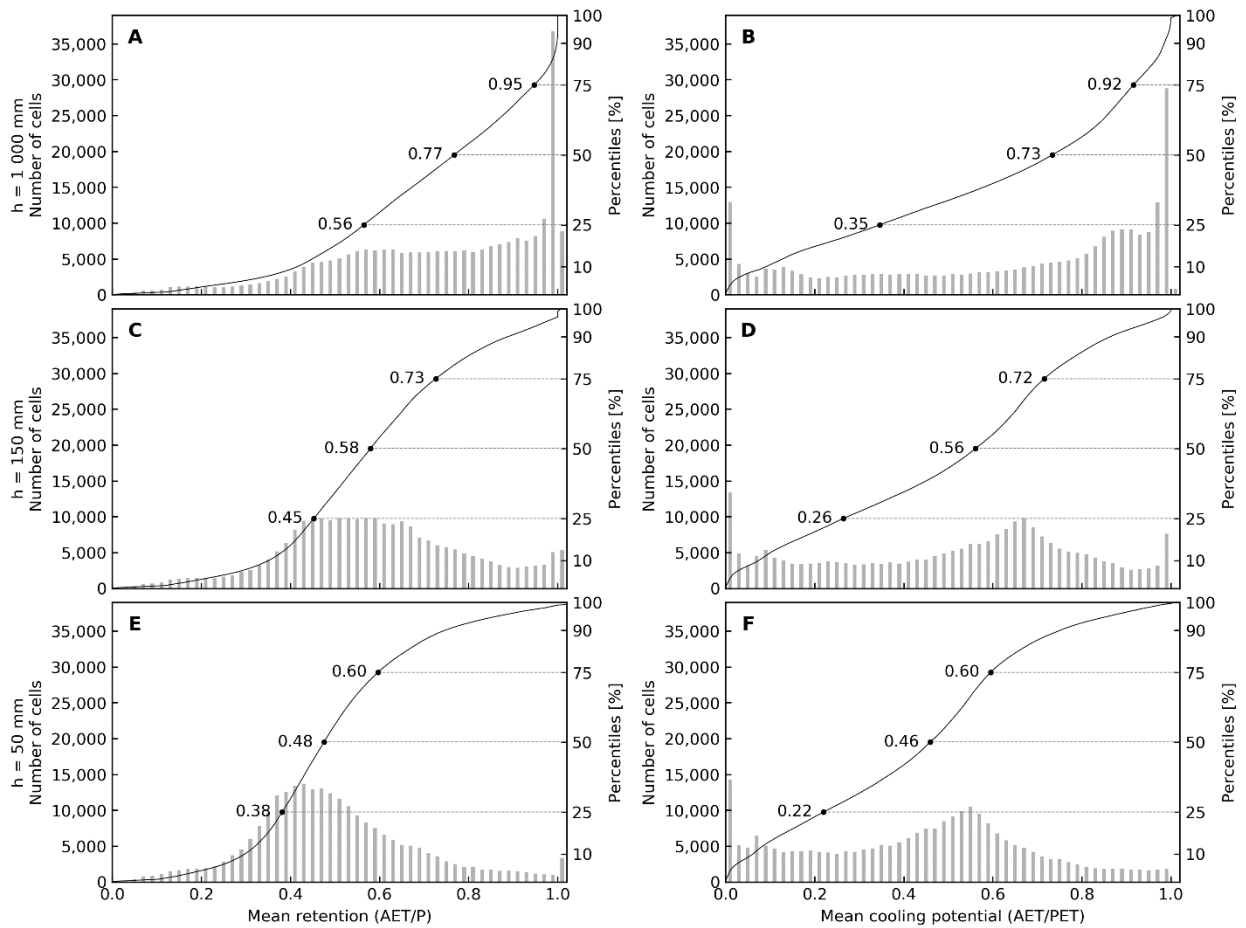
*Figure S8. Histograms of global mean retention and cooling potential for ERA5 forced simulations for (**A,B**) deep substrate (h = 1000 mm) (**C,D**) intensive substrate (h = 150 mm) (**E,F**) extensive substrate (h = 50 mm)*
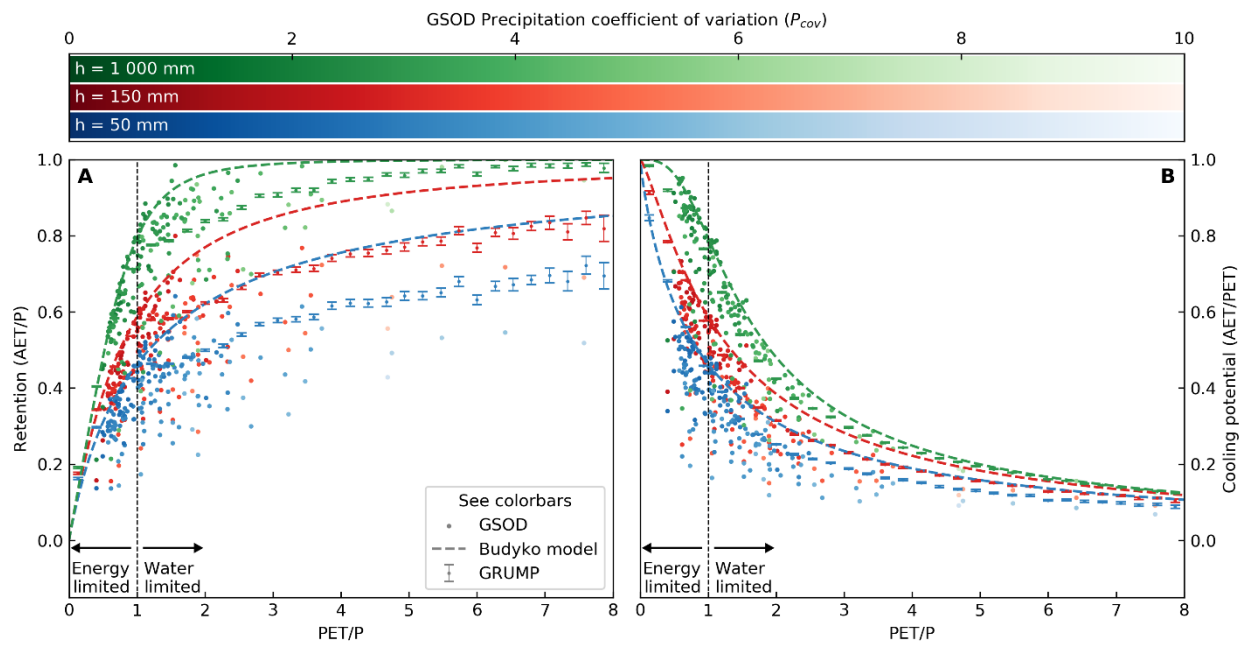
*Figure S9. Comparisons between modelled (**A**) retention and (**B**) cooling for GSOD and GRUMP locations. Upper bounding Budyko curves lambda values are 3, 1.3 and 0.9 for deep (h = 1000 mm), intensive (h = 150 mm), and extensive (h = 50 mm), substrate depths respectively. GRUMP values are mean values with error bars as SEM.*
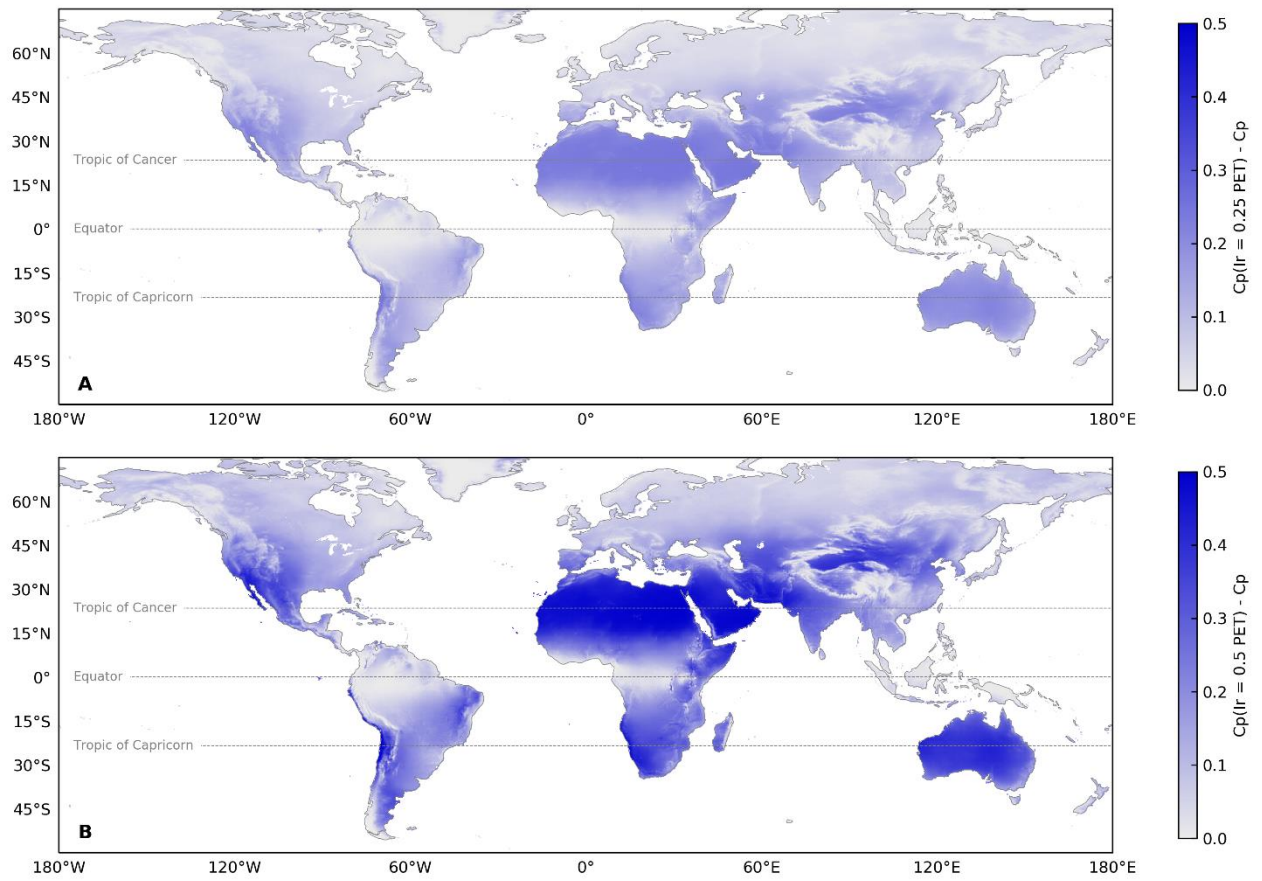
Figure S10. Global distribution of the change in cooling potential (CP) due to irrigation (Ir) scenarios for (A) irrigation equal to 25% of PET on non-rain days (B) irrigation equal to 50% of PET on non-rain days